PAPER • OPEN ACCESS

Turbulence spreading induced $E \times B$ vortex flow generation in a magnetic island

To cite this article: E.S. Yoon *et al* 2024 *Nucl. Fusion* **64** 126050

OPEN ACCESS
IOP Publishing | International Atomic Energy Agency
Nuclear Fusion
Nucl. Fusion **64** (2024) 126050 (8pp)
https://doi.org/10.1088/1741-4326/ad82fa

Turbulence spreading induced $E \times B$ vortex flow generation in a magnetic island

E.S. Yoon[1,*], T.S. Hahm[2,*], G.J. Choi[2], Y.W. Cho[3], A. Ishizawa[4], M.J. Choi[5] and J.M. Kwon[5]

[1] Department of Nuclear Engineering, Ulsan National Institute of Science and Technology, Ulsan 44919, Korea, Republic Of
[2] Nuclear Research Institute for Future Technology and Policy, Seoul National University, Seoul 08826, Korea, Republic Of
[3] School of Physical and Mathematical Sciences, Nanyang Technological University, Singapore 637371, Singapore
[4] Graduate School of Energy Science, Kyoto University, Uji, Kyoto 611-0011, Japan
[5] Korea Institute of Fusion Energy, Daejeon 34133, Korea, Republic Of

E-mail: esyoon@unist.ac.kr and tshahm@snu.ac.kr

Received 15 August 2024, revised 24 September 2024
Accepted for publication 3 October 2024
Published 16 October 2024

Abstract

We derive a self-consistent relation between turbulence spreading flux and vortex flow acceleration for time-stationary turbulence inside a magnetic island (MI) by extending the Charney-Drazin momentum theorem. The result, which consists of flux-surface-averaged expressions with geometrical weight, indicates a dominant balance between the turbulence spreading flux through regions around X-points and the vortex flow away from the X-points on the same flux surface. This is in qualitative agreement with experimental observations from DIII-D, KSTAR and HL-2A.

Keywords: momentum theorem, turbulence spreading, exb vortex flow, magnetic island, flow generation

(Some figures may appear in colour only in the online journal)

1. Introduction

One of the remaining challenges in understanding, predicting, and controlling turbulent transport in magnetic fusion plasmas is the multi-scale interaction between macroscopic structures and microturbulence. Interaction between the magnetic island (MI)-turbulence is a prime example of ongoing interest as reviewed [1–3].

A large MI caused by the tearing instability [4] usually deteriorates confinement and sometimes leads to a termination of plasma. Consequently, it attracts a considerable research interest regarding the successful operation of ITER [5]. It can also be produced by external perturbations [6] and has been utilized for the resonant magnetic perturbation induced control of the edge-localized magneto-hydrodynamic modes [7]. In addition, it can facilitate the formation of an internal transport barrier in stellarators [2]. Therefore, turbulence dynamics around MI is a fusion-relevant, rich, and theoretically challenging subject which requires a deeper understanding.

* Authors to whom any correspondence should be addressed.

An MI is known to modify the profiles around it. In most cases [1–3], profiles across the O-points become flattened inside the MI, while they become steeper just outside the separatrix. Microturbulence measurements indicate that the fluctuation amplitude gets reduced significantly inside an MI across the O-points, compared to the cases without an MI [8–12]. However, it is definitely maintained above the noise-level, while a local linear instability is not expected due to flattened profiles. This could be attributed to turbulence spreading [14–18] from outside the separatrix where the profiles get further steepened.

In addition, experimental measurements indicate the existence of $E \times B$ vortex flow circulating inside the MI [19]. $E \times B$ flow shear is well-known to regulate turbulence [20] and the geometric effects in an axisymmetric torus [21] can induce an in-out asymmetry of turbulence reduction behavior at the same flux surface as shown in experiments [22] and simulations [23]. It can also play an important role in nonlocal physics [24] including the turbulence spreading [25]. Motivated by this, there has been a recent publication addressing the spatial structure of the $E \times B$ shearing rate in MI [26] which could influence transport bifurcations in MI geometry [27]. The $E \times B$ zonal flows self-driven by turbulence [28] also exhibits similar shearing effects [29, 30]. In relation to this, the long term collisionless relaxation of the vortex flow in MI [31, 32] has been studied, extending the work [33] in an axisymmetric torus.

While numerical simulations show the vortex generation around the MI via Reynolds stress [1, 34], there has been no detailed analytic calculation to date taking the MI geometry into account. Reference [35] addressed the shear flow generation outside an MI only using the wave kinetics. One technical challenge of explicitly carrying out a vortex flow generation calculation, for instance, through a modulational instability [36–38], is properly representing the spatial structure of microturbulence inside an MI which is presumably not consisting of the linear eigenmodes, but being spread from outside.

Instead, in this work, we pursue a derivation of the self-consistent relation between the vortex flow acceleration and the turbulence spreading flux. This is an extension of the momentum theorem *à la* Charney-Drazin [39] to the MI geometry. The original work concerning the geophysical fluid dynamics (GFD) system is widely known in that community [40]. There have been a few publications addressing its possible applications to cases relevant to the magnetic fusion energy (MFE) [41–44].

The implications related to this work can be summarized as follows: For a 2D turbulence system which conserves the potential vorticity (PV) q, we have $\frac{\mathrm{d}}{\mathrm{d}t}q = 0$. One can derive a relation in a simple slab geometry that reads [41]

$$\frac{\partial}{\partial t}\langle u_y \rangle = -\left(\frac{\mathrm{d}\langle q \rangle}{\mathrm{d}x}\right)^{-1}\frac{\partial}{\partial x}\langle \delta q^2 \delta v_x \rangle + \cdots .$$

Here $\langle \cdots \rangle$ indicates a flux surface average, $\delta(\cdots)$ is a perturbed part, x is the direction of the profile inhomogeneity, and u is a flow. We have ignored the forcing, dissipation and assumed a time-stationary turbulence, i.e. $\frac{\partial}{\partial t}\langle \delta q^2 \rangle = 0$. This situation has been encountered in numerous global nonlinear gyrokinetic simulations in which local nonlinear saturation of turbulence occurs prior to ensuing turbulence spreading which accompanies zonal flow evolution. This assumption has also been used in previous theoretical investigations [41, 44]. This relation, after various simplifying assumptions, states that the zonal flow can be accelerated by the divergence of the turbulence spreading flux, more precisely the potential enstrophy flux. Its significance deserves more recognition in MFE in our opinion. In fact, there are a couple of new results on which this relation can provide an important insight [45, 46]. We discuss further details in the main text.

In this paper, we derive the momentum theorem in MI geometry based on a 2D PV-conserving drift wave system [44]. Our results relate the vortex flow acceleration in the MI to the turbulence spreading flux from outside of the MI, without assuming any linearly unstable mode inside the MI. Both terms appear with flux surface averaged expressions in the MI geometry which involve different weighting factors. There exists a dominant balance between the turbulence spreading flux through regions around the X-points and the vortex flow acceleration away from the X-points on the same flux surface. We note that the latter is a region where the flow measurements are feasible [11, 13, 19, 47], and the former's significance has been emphasized in both experiments [11, 13, 48] and theory [26]. Therefore, our results are consistent with the existing experimental results and will be useful in further detailed validations.

The remainder of this article is organized as follows: In section 2, we introduce our theoretical model. In section 3, we present a derivation of the momentum theorem in MI geometry. The implications of our results are included in section 4. Finally, section 5 contains further discussion.

2. Theoretical model

We consider a potential vorticity (PV) conserving 2D drift wave—zonal flow system [44] inside a static macroscopic MI. Neither the MI evolution in the presence of microturbulence [49] or MI effects on microinstability [50] are considered in this work. Inside an MI, a simple monopolar vortex plays the role of zonal flows in axisymmetric toroidal plasmas. We adopt a standard simple MI geometry [51] in which the equilibrium magnetic field is given by

$$\vec{B} = B_0\hat{z} + \frac{\overline{\delta\psi}}{R}\hat{z}\times\vec{\nabla}\Omega. \tag{1}$$

The parameter $\overline{\delta\psi}$ denotes the amplitude of the poloidal flux, $\delta\psi = \overline{\delta\psi}\cos\xi$, which induces a MI. This is assumed to be a constant, i.e. the constant-ψ approximation [4]. Here, $\xi = m\theta - n\zeta = m\left(\theta - \frac{\zeta}{q(r_s)}\right)$ is the helical angle coordinate, with $\theta - \frac{\zeta}{q(r_s)}$ being the angle along the axisymmetric equilibrium magnetic field. The coordinates ζ and θ represent the

toroidal and poloidal magnetic field directions, respectively, in the standard field-aligned coordinate system. We consider an axisymmetric equilibrium destroyed by a single-helicity static MI located at the rational surface r_s, where the local safety factor $q(r_s) = m/n$, and n and m are the toroidal and poloidal mode numbers, respectively. The major radius of the torus is denoted by R. The normalized flux function representing the MI is given by $\Omega = \frac{2(r-r_s)^2}{W^2} - \cos\xi$, where $W = 2\left(\frac{q}{\hat{s}}\frac{\overline{\delta\psi}}{B}\right)^{1/2}$ represents the island half-width, and $\hat{s}$ is the magnetic shear.

For analytic studies, it is natural to work in the polar coordinate (ρ, χ) [26]

$$\rho\cos\chi = x \tag{2}$$

$$\rho\sin\chi = W\sin\left(\frac{k_y}{2}y\right) \tag{3}$$

and

$$\rho^2 = \left(\frac{\Omega+1}{2}\right)W^2 = x^2 + W^2\sin^2\left(\frac{k_y}{2}y\right). \tag{4}$$

This is illustrated in figure 1.

Throughout this paper, we ignore the spatial variation of $|\vec{B}|$, and take $|\vec{B}| \simeq B_0 = \text{const}$. From now on, we drop the subscript '0' for notational simplicity.

The PV conservation equation reads

$$\frac{\partial}{\partial t}q + \vec{\nabla}\cdot(q\vec{u_E}) = 0, \tag{5}$$

where the PV is given by [44, 52]

$$q \equiv N\{1 + (\phi - \langle\phi\rangle)\} - \frac{1}{B^2}\vec{\nabla}_\perp\cdot\left(N\vec{\nabla}_\perp\phi\right). \tag{6}$$

Here, various dimensionless quantities are defined as

$$N(\vec{x}) = \frac{n_0(\vec{x})}{n_0}, \quad \phi(\vec{x}) = \frac{|e|\delta\phi(\vec{x})}{T_e}, \quad \vec{B}(\vec{x}) = \frac{\vec{B}_{\text{phys}}(\vec{x})}{B_0}.$$

Also, $\vec{\nabla}_\perp$ is a gradient perpendicular to the background magnetic field normalized by the inverse of $\rho_s \equiv c_s/\Omega_{ci} = (T_e/M_i)^{1/2}/(|e|B_0/M_i c)$, $\frac{\partial}{\partial t}$ is normalized to Ω_{ci}, $\vec{B}_{\text{phys}}(\vec{x})$ is the magnetic field in physical unit, and n_0 is a constant background density.

Equation (5) with equation (6) possesses two inviscid global invariants which consist of the energy and the enstrophy. In such systems, a dual cascade of turbulence occurs. Therefore, the energy can inverse-cascade to large scales and possibly lead to vortex formation.

3. Momentum theorem

In this section, we derive the momentum theorem or non-acceleration theorem [39] in an MI geometry. This has been widely known in the GFD community [40]. Its application to the MFE has been considered in [41, 43, 44]. We aim at deriving the conditions for acceleration of the flux-surface-averaged vortex flow.

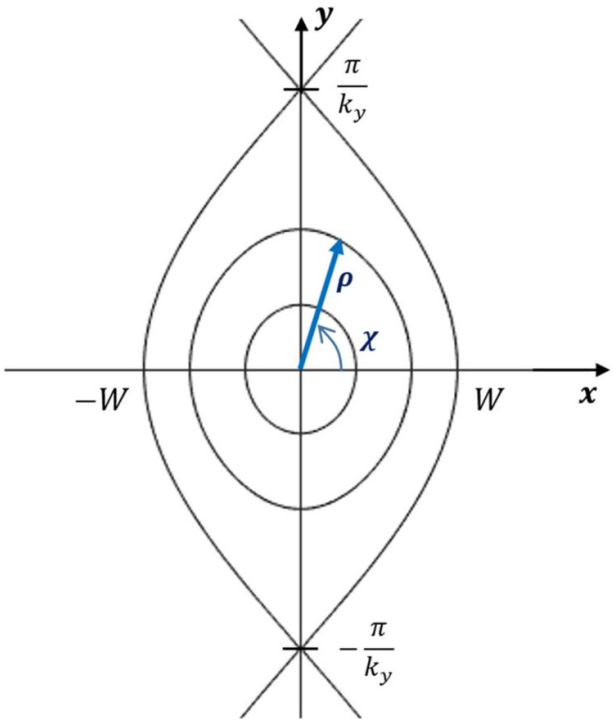

Figure 1. A simple MI model equilibrium and associated polar coordinate inside an MI. Reprinted from [26], with the permission of AIP Publishing.

From equations (1-4), we show that

$$\vec{B}_\perp \equiv \frac{\overline{\delta\psi}}{R}\hat{z}\times\vec{\nabla}\Omega = 4\frac{\overline{\delta\psi}}{RW^2}\rho\hat{z}\times\vec{\nabla}\rho, \tag{7}$$

and

$$\vec{B}_\perp\cdot\vec{\nabla} = \frac{4\overline{\delta\psi}}{R}\frac{\rho}{W^2}\left(\hat{z}\times\vec{\nabla}\rho\cdot\vec{\nabla}\chi\right)\frac{\partial}{\partial\chi}, \tag{8}$$

where

$$J^{-1} \equiv \hat{z}\times\vec{\nabla}\rho\cdot\vec{\nabla}\chi = \frac{k_y W}{2\rho}\sqrt{1-\left(\frac{\rho}{W}\right)^2\sin^2\chi}. \tag{9}$$

Here, J is the Jacobian of the coordinate transformation. Accordingly, we define the flux-surface-average as,

$$\langle A\rangle \equiv \frac{\oint \mathrm{d}\chi JA}{\oint \mathrm{d}\chi J}. \tag{10}$$

Now, the PV conservation equation (5) can be written as

$$\frac{\partial}{\partial t}\delta q + \vec{u}_E\cdot\vec{\nabla}\delta q + \vec{u}_E\cdot\vec{\nabla}\langle q\rangle = 0. \tag{11}$$

Here

$$\langle q\rangle \equiv N - \frac{1}{B^2}\langle\vec{\nabla}_\perp\cdot\left(N\vec{\nabla}_\perp\phi\right)\rangle \quad \text{and} \tag{12a}$$

$$\delta q = q - \langle q\rangle. \tag{12b}$$

Multiplying equation (11) by δq and flux-surface-averaging, we obtain

$$\frac{1}{2}\frac{\partial}{\partial t}\langle \delta q^2\rangle + \frac{1}{2}\langle \vec{\nabla}\cdot\left(\delta q^2 \vec{u}_E\right)\rangle + \langle \delta q \vec{u}_E\rangle\cdot\vec{\nabla}\langle q\rangle = 0. \tag{13}$$

By using the following identity in the MI-geometry,

$$\langle \vec{\nabla}\cdot\vec{A}\rangle \equiv \left\langle \frac{1}{J}\frac{\partial}{\partial\rho}\left(J\left(\vec{A}\cdot\vec{\nabla}\right)\rho\right)\right\rangle + \left\langle \frac{1}{J}\frac{\partial}{\partial\chi}\left(J\left(\vec{A}\cdot\vec{\nabla}\right)\chi\right)\right\rangle = \frac{\oint d\chi \frac{\partial}{\partial\rho} J\left(\vec{A}\cdot\vec{\nabla}\right)\rho}{\oint d\chi J}. \tag{14}$$

Equation (13) can be made more explicit,

$$\frac{1}{2}\frac{\partial}{\partial t}\langle \delta q^2\rangle + \frac{1}{2}\left(\oint \mathrm{d}\chi J\right)^{-1}\frac{\partial}{\partial\rho}\left[\oint \mathrm{d}\chi J \delta q^2 \vec{u}_E\cdot\vec{\nabla}\rho\right] + \left(\oint \mathrm{d}\chi J\right)^{-1}\oint \mathrm{d}\chi\left(J\delta q\vec{u}_E\cdot\vec{\nabla}\rho\right)\frac{\partial}{\partial\rho}\langle q\rangle. \tag{15}$$

On the other hand, the flux-averaged part of equation (5) yields

$$\frac{\partial}{\partial t}\frac{1}{B^2}\langle \vec{\nabla}_\perp\cdot\left(N\vec{\nabla}_\perp\phi\right)\rangle = \langle\vec{\nabla}\cdot\left(\delta q\vec{u}_E\right)\rangle. \tag{16}$$

Here, we have used the fact that $\langle\vec{\nabla}\cdot\left(\langle q\rangle\vec{u}_E\right)\rangle = 0$, since

$$\vec{u}_E \equiv \frac{-\vec{\nabla}\phi\times\hat{z}}{B} = \frac{1}{B}\left(\frac{\partial\Phi}{\partial\rho}\right)\hat{z}\times\vec{\nabla}\rho - \frac{1}{B}\left(\frac{\partial\Phi}{\partial\chi}\right)\hat{z}\times\vec{\nabla}\chi$$

leads to $\vec{\nabla}\cdot\vec{u}_E = 0$ and $\langle\vec{u}_E\cdot\vec{\nabla}\rho\rangle = 0$.

Once again, using equation (14), we can write equation (16) as

$$\frac{\partial}{\partial t}\frac{\partial}{\partial\rho}\left\{\frac{N}{B^2}\oint \mathrm{d}\chi\left(J\vec{\nabla}\Phi\cdot\vec{\nabla}\rho\right)\right\} = \frac{\partial}{\partial\rho}\oint \mathrm{d}\chi\left(J\delta q\vec{u}_E\cdot\vec{\nabla}\rho\right). \tag{17}$$

Integrating once in ρ, we obtain

$$\frac{\partial}{\partial t}\oint \mathrm{d}\chi\frac{N}{B^2}J\left(\vec{\nabla}\Phi\cdot\vec{\nabla}\rho\right) = \oint \mathrm{d}\chi\left(J\delta q\vec{u}_E\cdot\vec{\nabla}\rho\right). \tag{18}$$

Following [44], we assume that the constant of integration vanishes. This needs to be modified if we consider the effect of an external (imposed) electric field. However, it is beyond the scope of this work.

Finally, by eliminating '$\oint \mathrm{d}\chi J\delta q\vec{u}_E\cdot\vec{\nabla}\rho$' from equations (15) and (18), we obtain

$$\frac{\partial}{\partial t}\left[\oint \mathrm{d}\chi\frac{N}{B^2}J\left(\vec{\nabla}\Phi\cdot\vec{\nabla}\rho\right) + \frac{\oint \mathrm{d}\chi J\langle\delta q^2\rangle}{2\frac{\partial}{\partial\rho}\langle q\rangle}\right] = -\frac{1}{2\frac{\partial}{\partial\rho}\langle q\rangle}\frac{\partial}{\partial\rho}\left[\oint \mathrm{d}\chi\left\{J\delta q^2\left(\vec{u}_E\cdot\vec{\nabla}\right)\rho\right\}\right]. \tag{19}$$

This is the desired momentum theorem in MI geometry. It is not totally surprising that equation (19) looks similar to equation (35) of [44] in shaped tokamak geometry. Despite obvious differences, there exist geometric similarities between the interior of an MI and the diverted tokamak geometry. These have been exploited in both ways [53, 54]. The first term in the bracket on the LHS is related to the angular component of the $E\times B$ vortex flow as will be discussed in the next section. The second term is the drift wave activity density (the negative of pseudo-momentum). The RHS of equation (19) is the divergence of the potential enstrophy density radial flux. This can be related to turbulence spreading or avalanches [24]. Equation (19) states that the vortex flow momentum is locked to the wave momentum density in the absence of forcing, dissipation (which are ignored in this work) and the potential enstrophy flux [41]. In other words, in the absence of forcing, dissipation, and turbulence spreading, stationary turbulence cannot accelerate a flux-surface-averaged vortex flow (note that the second term vanishes for stationary turbulence).

The momentum theorem's relevance to drift wave—zonal flow system in MFE has been discussed in a simple slab geometry [41] and has been further extended to an axisymmetric tokamak [44]. A recent example for which the momentum theorem can provide useful insight is a global nonlinear gyrokinetic simulation which indicates that turbulence spreading carries zonal flows alongside [45]. Finally, a somewhat counter-intuitive experimental trend [46] that plasmas with large avalanches are more likely to exhibit the $E\times B$ staircases as well, which can be understood from the fact that the $E\times B$ zonal flow can be accelerated by the turbulence spreading. As emphasized in a review article on the meso-scopic phenomena [24], a clear theoretical distinction between turbulence spreading and the avalanche is difficult.

While we have presented some details of the assumptions and approximations in this section, it would be useful at this juncture to add speculations on how various neglected effects could affect the key expression presented in equation (19). First, inhomogeneity of $|\mathbf{B}|$ in toroidal plasma which has been ignored could have been kept by introducing the magnetic potential vorticity as done in [44, 52]. Even though it would make the $E\times B$ flow compressible, a derivation similar to that of [44] would have led to an expression similar to equation (19), consisting of only three terms. The main difference would be that each term becomes more complex with geometric weighting so that their relation to experimentally measurable quantities are not simple. Such examples can be found in section IV of [44]. Of course, if one pursued a further physical characterization of the PV flux, one would have obtained an additional term [52], familiar from the turbulence equipartition pinch of toroidal angular momentum [55, 56]. Second, if we consider a finite ion temperature with $\frac{T_i}{T_e} = O(1)$, the PV conservation becomes no longer obvious, and an additional term proportional to $\vec{\nabla}B\times\vec{\nabla}\delta T_i$ appears [52]. Such correction term is related to baroclinic effects and is well known in GFD [40].

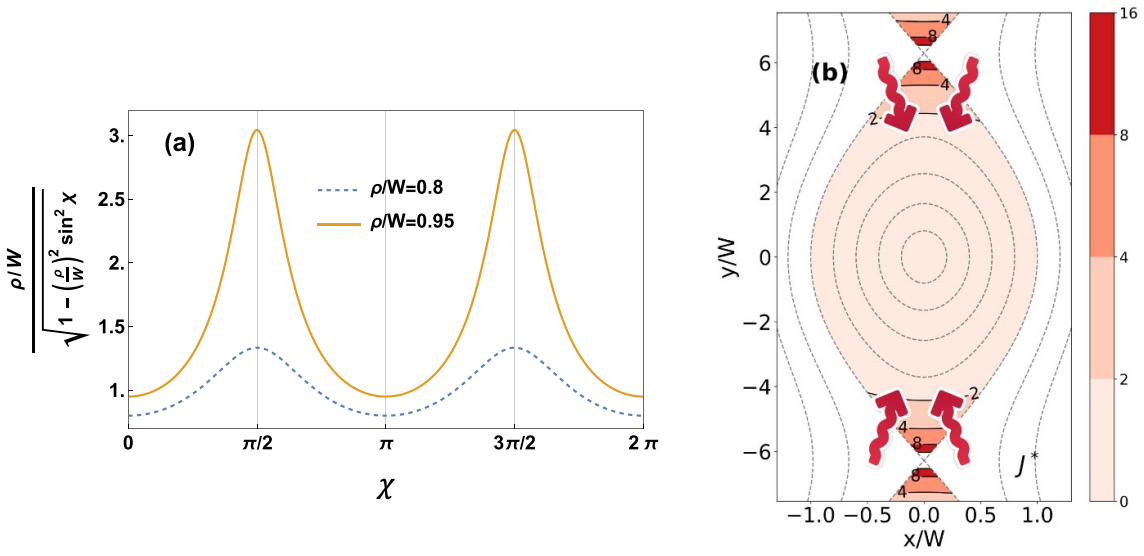

Figure 2. (*a*) χ-variation of $J^* \equiv \frac{\rho/W}{\sqrt{1-\left(\frac{\rho}{W}\right)^2 \sin^2\chi}}$ for $\frac{\rho}{W} = (0.8, 0.95)$ and (*b*) 2D structure of weighting function J^* for turbulence spreading in $k_y W = 0.5$ MI. Note a singularity at X-points.

4. Implication of momentum theorem on the vortex flow in a magnetic island

In this section, we discuss further quantitative details of the non-acceleration theorem in equation (19). Turbulence spreading flux on the RHS is proportional to $\oint \mathrm{d}\chi \{J\delta q^2(\vec{u}_E \cdot \vec{\nabla})\rho\}$. Since $J \propto \frac{\rho/W}{\sqrt{1-\left(\frac{\rho}{W}\right)^2 \sin^2\chi}}$, the turbulence spreading flux contribution to equation (19) is heavily weighted by contributions from the region around the X-points $(\rho, \chi) \simeq \left(W, \pm\frac{\pi}{2}\right)$ where J is very large. In fact, it exhibits an integrable singularity. Figure 2 illustrates the variations of J as a function of χ for different values of ρ/W. It is noteworthy that this observation is compatible with the experimental findings from DIII-D [11], KSTAR [13], and HL-2A [48] that turbulence spreading into an MI from outside mainly occurs through the regions near the X-points.

The first term in the LHS of equation (19) is related to the vortex flow around an MI. Since $\vec{\nabla}\Phi \cdot \vec{\nabla}\rho = \left(\frac{\partial\Phi}{\partial\rho}\right)|\vec{\nabla}\rho|^2 + \left(\frac{\partial\Phi}{\partial\chi}\right)\vec{\nabla}\chi \cdot \vec{\nabla}\rho$, we can write

$$\oint \mathrm{d}\chi J\vec{\nabla}\Phi \cdot \vec{\nabla}\rho = \oint \mathrm{d}\chi J|\vec{\nabla}\rho|^2 \left(\frac{\partial\Phi}{\partial\rho}\right) + \oint \mathrm{d}\chi \left(J\vec{\nabla}\chi \cdot \vec{\nabla}\rho\right)\left(\frac{\partial\Phi}{\partial\chi}\right). \quad (20)$$

Note that the first term on the RHS is proportional to the χ-component of the $E \times B$ vortex flow because

$$\left(\frac{\partial\Phi}{\partial\rho}\right) = JB\left(\vec{u}_E \cdot \vec{\nabla}\right)\chi.$$

Figure 3 exhibits a χ-variation of $J|\vec{\nabla}\rho|^2$ for different values of ρ/W and $k_y W$. It exhibits broad maxima near $\chi \simeq 0, \pi$, i.e. near the mid-plane of an MI. This implies that the first term on the RHS of equation (20) is more heavily weighted by contributions near the mid-plane of an MI. This is the region where the experimental measurements [19, 57] of flows are relatively feasible, and the incompressible $E \times B$ vortex flow is expected to be stronger than that in the region near the X-points [13, 26, 58]. For a simple mono-polar vortex flow with $\Phi = \Phi(\rho)$, the second term on the RHS of equation (20) vanishes. This structure has been shown to persist [31] at least as well as the Rosenbluth-Hinton residual zonal flows [33] in an axisymmetric toroidal plasma under the long term enhancement of polarization shielding due to ion bounce motion [59]. While a more spatially complex non-monopolar vortex flow may be generated from a longer term neoclassical toroidal precession drift effect when the MI is not fat enough, [31] or when the MI is in a growing phase [34, 60], a quantification of effects from such structures is beyond the scope of this work. The second term on the LHS vanishes for stationary turbulence as mentioned before.

Finally, the RHS of equation (19) has a factor

$$\frac{\partial}{\partial\rho}\langle q\rangle = \frac{\partial}{\partial\rho}N - \frac{1}{B^2}\frac{\partial}{\partial\rho}\langle\vec{\nabla}\cdot N\vec{\nabla}\Phi\rangle \quad (21)$$

in the denominator. Since $\frac{\partial N}{\partial\rho}$ term dominates in the case of axisymmetric tokamak, the rest is often ignored [44]. However, inside an MI, this simplification may not be justified. Experimental measurements of the profiles have been rare [8, 9, 12, 58, 61–63] and simulation results vary [34, 64–72]. It is noteworthy that flux-driven fluid simulations observe turbulence inside an MI despite partially flattened profiles [1, 34]. We do not make further simplifications of that expression. Obviously, our theory does not assume any linearly unstable drift waves inside an MI, and can provide insights for the case in its absence. Due to its dependence on $\left[\frac{\partial}{\partial\rho}\langle q\rangle\right]^{-1}$, one

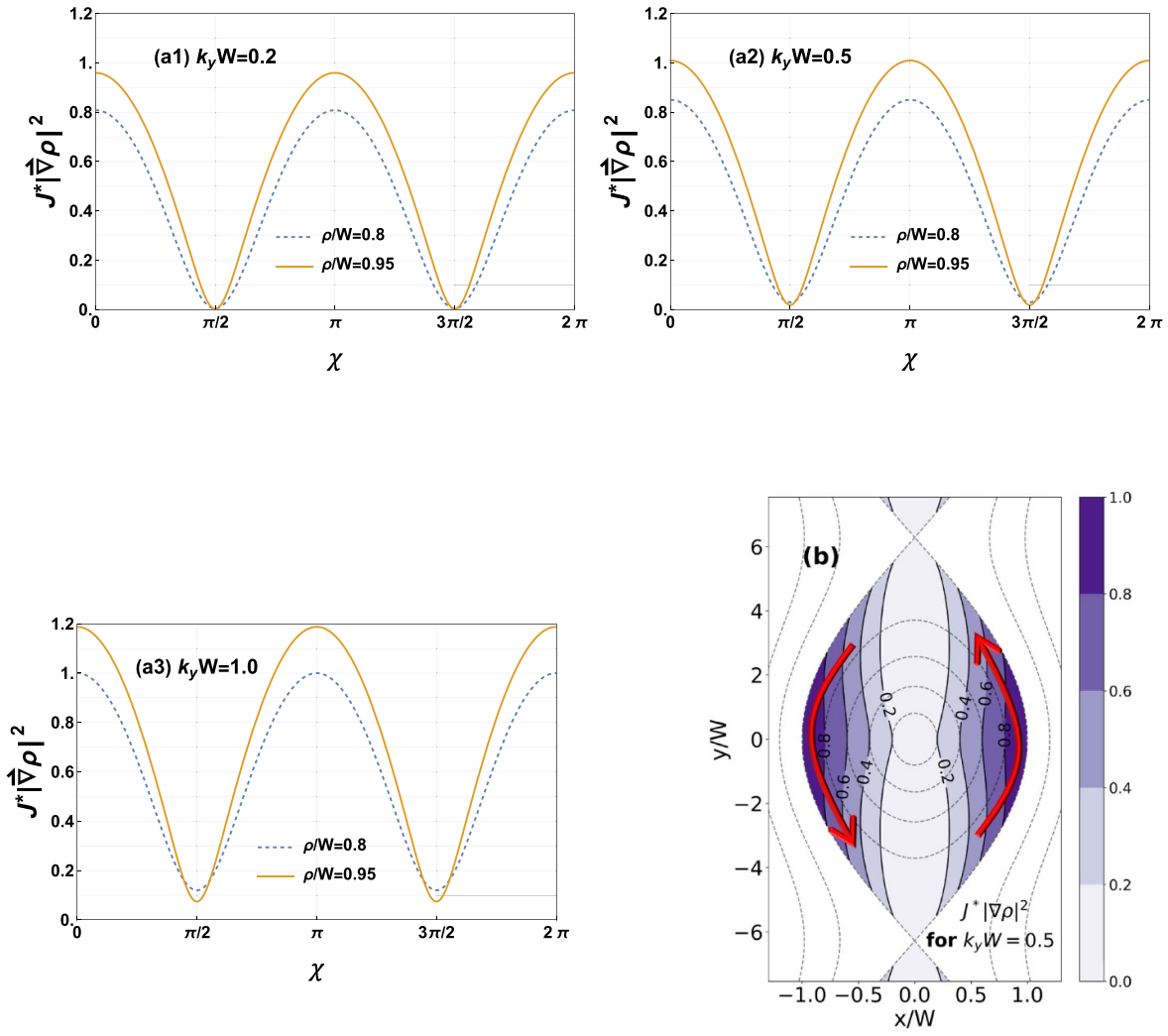

Figure 3. (*a*) χ-variation of $J^*|\nabla\rho|^2 = \frac{\rho/W}{\sqrt{1-\left(\frac{\rho}{W}\right)^2\sin^2\chi}}(\cos^2\chi + \rho^2 J^{-2}\sin^2\chi)$ for $\frac{\rho}{W} = (0.8, 0.95)$ and $k_yW = (0.2, 0.5, 1.0)$ and (*b*) 2D structure of weighting function $J^*|\nabla\rho|^2$ for the vortex flow.

may be tempted to conclude that turbulence spreading effects are enhanced for a very mild gradient of $\langle q\rangle$, or oft-quoted flattened profiles. However, a small $\frac{\partial}{\partial\rho}\langle q\rangle$ will probably result in a small perturbed PV, δq and therefore a small enstrophy flux [41]. We expect that our conclusion is relatively insensitive to the degree of profile flattening inside an MI. A particular case of $\frac{\partial}{\partial\rho}\langle q\rangle = 0$ is beyond the scope of this paper though.

5. Discussion

In relation to a previous work, [26] emphasized that the anisotropic $E\times B$ shearing rate associated with a vortex flow inside an MI makes turbulence spreading into the MI more feasible through the regions near the X-points. This work focused on only one aspect of the problem, i.e. through which regions of the MI the turbulence can penetrate more efficiently for a given $E\times B$ vortex structure. It does not address how the $E\times B$ vortex can be generated inside the MI, in particular, when there is no linearly unstable mode.

On the other hand, this work produces a self-consistent relation between the turbulence spreading flux and the vortex flow acceleration inside the MI. While no details of dynamical processes are provided in this approach, it nevertheless exhibits the possibility that the $E\times B$ vortex flow inside the MI can be generated from nonlocal effects such as turbulence spreading even when the local stability picture indicates the absence of any linearly unstable modes there. Indeed, the region around an MI is the place where the nonlocal behavior of turbulence [24] such as turbulence spreading can be prominent because of the spatial proximity of the linearly unstable region from the stable region.

An alternative approach might be a modulational instability calculation based on Reynolds stress [28, 36–38]. However, in the absence of linearly unstable modes, the specification of the primary (test) drift wave becomes too arbitrary. Instead, one might imagine a formulation involving a drift wave packet

which propagates from outside the MI. Finally, the profiles can steepen just outside the MI separatrix and turbulence developed from linearly unstable modes can generate the $E \times B$ flows [35]. While this can affect the $E \times B$ vortex flow inside the MI in principle, carrying out a credible calculation of such remains a challenge.

Our results indicate an intricate relation between turbulence spreading and macroscopic vortex generation. The former is expected to be most pronounced in the region where the fluctuation intensity profile variation is significant and the $E \times B$ shearing effect is weaker. Obviously, this can happen in the region around the X-points as the experiments [11, 13], simulations [65–71], and theory [26] indicates. On the other hand, the latter often involves the inverse cascade of energy due to nonlinear interactions of turbulent eddies. This process is, of course, expected to be efficient in the region where the fluctuation intensity is considerable. Its experimental validation should be possible since there has been a bicoherence analysis investigating turbulence-MI interaction [13].

While these two processes of turbulence spreading and inverse cascade of energy occur simultaneously, as emphasized in [17], our results are easier to understand heuristically by a sequence of turbulence spreading through the X-point region followed by an inverse transfer of energy to a macroscopic scale inside an MI. An alternate scenario includes a global (including the regions both outside and inside of an MI) inverse cascade of drift wave turbulence which favors the generation of a 'vortex mode' around the MI [73, 73] presented a radial eigenmode solution of the vortex mode (with the same helicity as that of the MI) around the tearing mode resistive layer. In principle, its extension to the case of a thick macroscopic MI can provide a useful theoretical insight into the vortex structure around the MI, which the momentum theorem derived in this work alone cannot provide. In addition, an extension to 2D magnetic turbulence would be worth pursuing.

Finally, an interplay between turbulence spreading and $E \times B$ flow shear also plays a prominent role in heat load broadening for power handling [74–81] which is an outstanding fusion-relevant problem. Implications of the momentum theorem in scrape-off layer geometry should be worth exploring in the future.

Acknowledgment

TSH acknowledges useful interactions on the subject with P.H. Diamond, Lu Wang, K. Ida, M. Jiang, S. M. Yi, M. Leconte, and E. Poli. This work was supported by Korea Hydro & Nuclear Power Co. (2021), the National Research Foundation of Korea (NRF) funded by the Korea government(Ministry of Science and ICT) (Grant No. 2023R1A2C100773512 and RS-2022-00155991), the Korea Institute of Energy Technology Evaluation and Planning and the Ministry of Trade, Industry & Energy (MOTIE) of the Republic of Korea (Grant No. 20214000000410), the R&D Program of the Korea Institute of Fusion Energy (KFE) funded by the Ministry of Science and ICT of the Republic of Korea (KFE-EN2441-10), and the Japanese Ministry of Education, Culture, Sports, Science and Technology (Grant No. 17K06991).

ORCID iDs

E.S. Yoon https://orcid.org/0000-0001-7107-7302
T.S. Hahm https://orcid.org/0000-0001-7015-0547
G.J. Choi https://orcid.org/0000-0003-0044-1650
Y.W. Cho https://orcid.org/0000-0001-6408-9604
A. Ishizawa https://orcid.org/0000-0002-5323-8448
M.J. Choi https://orcid.org/0000-0002-2825-6484
J.M. Kwon https://orcid.org/0000-0002-2300-152X

References

[1] Ishizawa A., Kishimoto Y. and Nakamura Y. 2019 *Plasma Phys. Control. Fusion* **61** 054006
[2] Ida K. 2020 *Plasma Phys. Control. Fusion* **62** 014008
[3] Choi M.J. 2021 *Rev. Mod. Plasma Phys.* **5** 9
[4] Furth H.P., Killeen J. and Rosenbluth M.N. 1963 *Phys. Fluids* **6** 459
[5] Turco F., Luce T.C., Solomon W., Jackson G., Navratil G.A. and Hanson J.M. 2018 *Nucl. Fusion* **58** 106043
[6] Hahm T.S. and Kulsrud R.M. 1985 *Phys. Fluids* **28** 2412
[7] Evans T.E. 2015 *Plasma Phys. Control. Fusion* **57** 123001
[8] Yu C. *et al* 1992 *Nucl. Fusion* **32** 1545
[9] Zhao K.J. *et al* 2015 *Nucl. Fusion* **55** 073022
[10] Bardóczi L., Rhodes T.L., Carter T.A., Bañón Navarro A., Peebles W.A., Jenko F. and McKee G. 2016 *Phys. Rev. Lett.* **116** 215001
[11] Ida K., Kobayashi T., Ono M., Evans T.E., McKee G.R. and Austin M.E. 2018 *Phys. Rev. Lett.* **120** 245001
[12] Jiang M. *et al* (HL-2A Team) 2018 *Nucl. Fusion* **58** 026002
[13] Choi M.J. *et al* 2021 *Nat. Commun.* **12** 375
[14] Garbet X., Laurent L., Samain A. and Chinardet J. 1994 *Nucl. Fusion* **34** 963
[15] Hahm T.S., Diamond P.H., Lin Z., Itoh K. and Itoh S.-I. 2004 *Plasma Phys. Control. Fusion* **46** A323
[16] Lin Z. and Hahm T.S. 2004 *Phys. Plasmas* **11** 1099
[17] Gurcan O. D., Diamond P.H., Hahm T.S. and Lin Z. 2005 *Phys. Plasmas* **12** 032303
[18] Hahm T.S., Diamond P.H., Lin Z., Rewoldt G., Gurcan O. and Ethier S. 2005 *Phys. Plasmas* **12** 090903
[19] Estrada T., Ascasíbar E., Blanco E., Cappa A., Hidalgo C., Ida K., López-Fraguas A. and Ph van Milligen B. 2016 *Nucl. Fusion* **56** 026011
[20] Biglari H., Diamond P.H. and Terry P.W. 1990 *Phys. Fluids* B **2** 1–4
[21] Hahm T.S. and Burrell K.H. 1995 *Phys. Plasmas* **2** 1648
[22] Rettig C.L., Peebles W.A., Burrell K.H., La Haye R.J., Doyle E.J., Groebner R.J. and Luhmann N.C. Jr 1993 *Phys. Fluids* B **5** 2428
[23] Cho Y.W., Yi S., Kwon J.M. and Hahm T.S. 2016 *Phys. Plasmas* **23** 102312
[24] Hahm T.S. and Diamond P.H. 2018 *J. Korean Phys. Soc.* **73** 747–92
[25] Wang W.X., Hahm T.S., Lee W.W., Rewoldt G., Manickam J. and Tang W.M. 2007 *Phys. Plasmas* **14** 072306
[26] Hahm T.S., Kim Y.J., Diamond P.H. and Choi G.J. 2021 *Phys. Plasmas* **28** 022302
[27] Guo W., Jiang M., Diamond P.H., Chen C.-C., Cao M., Li H. and Long T. 2022 *Plasma Phys. Control. Fusion* **64** 124001
[28] Diamond P.H., Itoh S.-I., Itoh K. and Hahm T.S. 2005 *Plasma Phys. Control. Fusion* **47** R35
[29] Lin Z., Hahm T.S., Lee W., Tang W.M. and White R.B. 1998 *Science* **281** 1835

[30] Hahm T.S., Beer M.A., Lin Z., Hammett G.W., Lee W.W. and Tang W.M. 1999 *Phys. Plasmas* **6** 922
[31] Choi G.J. and Hahm T.S. 2022 *Phys. Rev. Lett.* **128** 225001
[32] Choi G.J. 2023 *Nucl. Fusion* **63** 066032
[33] Rosenbluth M.N. and Hinton F.L. 1998 *Phys. Rev. Lett.* **80** 724
[34] Ishizawa A. and Nakajima N. 2009 *Nucl. Fusion* **49** 055015
[35] Leconte M. and Cho Y.W. 2023 *Nucl. Fusion* **63** 034002
[36] Diamond P.H., Rosenbluth M.N., Hinton F.L., Malkov M., Fleischer J. and Smolyakov A. 1998 *Plasma Physics and Controlled Nuclear Fusion Research, 18th IAEA Energy Conf., Yokohama,Japan (Int. Atomic Energy Agency, Vienna) (paper No. IAEACN-69/TH3/1)*
[37] Chen L., Lin Z. and White R. 2000 *Phys. Plasmas* **7** 3129
[38] Hahm T.S., Choi G.J., Park S.J. and Na Y.-S. 2023 *Phys. Plasmas* **30** 072501
[39] Charney J.G. and Drazin P.G. 1961 *J. Geophys. Res.* **66** 83–109
[40] Vallis G.K. 2017 *Atmospheric and Oceanic Fluid Dynamics* 2nd edn (Cambridge University Press)
[41] Diamond P.H., Gurcan O.D., Hahm T.S., Miki K., Kosuga Y. and Garbet X. 2008 *Plasma Phys. Control. Fusion* **50** 124018
[42] Kosuga Y., Diamond P.H., Wang L., Gürcan O..D. and Hahm T.S. 2013 *Nucl. Fusion* **53** 043008
[43] Gürcan O..D. and Diamond P.H. 2015 *J. Phys. A: Math. Theor.* **48** 293001
[44] Hahm T.S., Diamond P.H., Park S.J. and Na Y.-S. 2024 *Phys. Plasmas* **31** 032310
[45] Yi S., Sung C., Yoon E.S., Kwon J.-M., Hahm T.S., Kim D., Kang J. J., Cho Y.W. and Qi L. 2024 *Phys. Plasmas* **31** 022307
[46] Choi M.J. *et al* 2024 *Plasma Phys. Control. Fusion* **66** 065013
[47] Ida K. *et al* 2004 *Nucl. Fusion* **44** 290
[48] Li Y.C. *et al* HL-2A 2023 *Sci. Rep.* **13** 4785
[49] Ishizawa A. and Waelbroeck F.L. 2013 *Phys. Plasmas* **20** 122301
[50] Zhang G., Guo W. and Wang L. 2022 *Plasma Phys. Control. Fusion* **64** 045006
[51] Rutherford P.H. 1973 *Phys. Fluids* **16** 1903
[52] McDevitt C.J., Diamond P.H., Gürcan O. D. and Hahm T.S. 2010 *Phys. Plasmas* **17** 112509
[53] Hahm T.S. and Diamond P.H. 1987 *Phys. Fluids* **30** 133–43
[54] Biancalani A., Chen L., Pegoraro F. and Zonca F. 2010 *Phys. Rev. Lett.* **105** 095002
[55] Hahm T.S., Diamond P.H., Gurcan O.D. and Rewoldt G. 2007 *Phys. Plasmas* **14** 072302
[56] Gürcan O.D., Diamond P.H. and Hahm T.S. 2008 *Phys. Rev. Lett.* **100** 135001
[57] Ida K. *et al (LHD Experimental Group)* 2001 *Phys. Rev. Lett.* **88** 015002
[58] Choi M.J. *et al* 2017 *Nucl. Fusion* **57** 126058
[59] Fong B.H. and Hahm T.S. 1999 *Phys. Plasmas* **6** 188–99
[60] Zhao K.J. *et al* 2017 *Nucl. Fusion* **57** 126006
[61] de Vries P.C., Waidmann G., Kramer-Flecken A., Donne A.J.H. and Schuller F.C. 1997 *Plasma Phys. Control. Fusion* **39** 439
[62] Ida K., Kobayashi T., Evans T.E., Inagaki S., Austin M.E., Shafer M.W., Ohdachi S., Suzuki Y., Itoh S.-I. and Itoh K. 2015 *Sci. Rep.* **5** 16165
[63] Bardóczi L., Rhodes T.L., Bañón Navarro A., Sung C., Carter T.A., La Haye R.J., McKee G.R., Petty C.C., Chrystal C. and Jenko F. 2017 *Phys. Plasmas* **24** 056106
[64] Poli E., Bottino A. and Peeters A.G. 2009 *Nucl. Fusion* **49** 075010
[65] Hornsby A., Peeters A.G., Snodin A.P., Casson F.J., Camenen Y., Szepesi G., Siccinio M. and Poli E. 2010 *Phys. Plasmas* **17** 092301
[66] Bañón Navarro A., Bardóczi L., Carter T.A., Jenko F. and Rhodes T.L. 2017 *Plasma Phys. Control. Fusion* **59** 034004
[67] Kwon J.-M., Ku S., Choi M.J., Chang C.S., Hager R., Yoon E.S., Lee H.H. and Kim H.S. 2018 *Phys. Plasmas* **25** 052506
[68] Kwon J.M., Ku S., Chang C.S., Choi M.J., Hager R., Yoon E.S., Lee H.H. and Kim H.S. 2018 *27th IAEA Fusion Energy Conf. (Gandhinagar, India FEC)* p TH/8-1
[69] Fang K.S. and Lin Z. 2019 *Phys. Plasmas* **26** 052510
[70] Fang K., Bao J. and Lin Z. 2019 *Plasma Sci. Technol.* **21** 115102
[71] Muto M., Imadera K. and Kishimoto Y. 2022 *Phys. Plasmas* **29** 052503
[72] Tae W., Yoon E.S., Hur M.S., Choi G.J., Kwon J.M. and Choi M.J. 2024 *Phys. Plasmas* **24** 020702
[73] McDevitt C.J. and Diamond P.H. 2006 *Phys. Plasmas* **13** 032302
[74] Chu X., Diamond P.H. and Guo Z. 2022 *Nucl. Fusion* **62** 066021
[75] Kobayashi M., Tanaka K., Ida K., Hayashi Y., Takemura Y. and Kinoshita T. 2022 *Phys. Rev. Lett.* **128** 125001
[76] Wu T. *et al* 2023 *Nucl. Fusion* **63** 126001
[77] Diamond P.H., Chu X., Cao M., Wu T. and Guo Z.B. 2023 *29th IAEA Fusion Energy Conf., (London, United Kingdom, IAEA-CN-316- 1777 FEC)*
[78] Li N., Xu X.Q., Diamond P.H., Zhang T., Liu X., Wang Y.F., Yan N. and Xu G.S. 2023 *Nucl. Fusion* **63** 124005
[79] Kin F. *et al* 2023 *Phys. Plasmas* **30** 112505
[80] Li Z., Chen X.I., Diamond P.H., Xu X., Qin X., Wang H., Scotti F., Hong R., Yu G., Yan Z., Filipp K. and George R. M. 2024 *Commun. Phys.* **7** 96
[81] Long T. *et al* 2024 *Nucl. Fusion* **64** 064002